

Flavor stability analysis of dense supernova neutrinos with flavor-dependent angular distributions

Alessandro Mirizzi¹ and Pasquale Dario Serpico²

¹*II Institut für Theoretische Physik, Universität Hamburg,
Luruper Chaussee 149, 22761 Hamburg, Germany*

²*LAPTh, Univ. de Savoie, CNRS, B.P.110, Annecy-le-Vieux F-74941, France*

Numerical simulations of the supernova (SN) neutrino self-induced flavor conversions, associated with the neutrino-neutrino interactions in the deepest stellar regions, have been typically carried out assuming the “bulb-model”. In this approximation, neutrinos are taken to be emitted half-isotropically by a common neutrinosphere. In the recent Ref. [1] we have removed this assumption by introducing flavor-dependent angular distributions for SN neutrinos, as suggested by core-collapse simulations. We have found that in this case a novel multi-angle instability in the self-induced flavor transitions can arise. In this work we perform an extensive study of this effect, carrying out a linearized flavor stability analysis for different SN neutrino energy fluxes and angular distributions, in both normal and inverted neutrino mass hierarchy. We confirm that spectra of different ν species which cross in angular space (where $F_{\nu_e} = F_{\nu_x}$ and $F_{\bar{\nu}_e} = F_{\bar{\nu}_x}$) present a significant enhancement of the flavor instability, and a shift of the onset of the flavor conversions at smaller radii with respect to the case of an isotropic neutrino emission. We also illustrate how a qualitative (and sometimes quantitative) understanding of the dynamics of these systems follows from a stability analysis.

PACS numbers: 14.60.Pq, 97.60.Bw

I. INTRODUCTION

Flavor conversions of neutrinos emitted from core-collapse supernovae (SNe) represent a diagnostic tool to get crucial information about their mixing parameters and the SN dynamics in the deepest stellar regions [2]. In particular, SNe are a unique laboratory to probe neutrino oscillations in extreme conditions. Supernova neutrinos can interact not only with the stellar medium via the Mikheyev-Smirnov-Wolfenstein (MSW) effect [3, 4], but also with other neutrinos (ν) and antineutrinos ($\bar{\nu}$) as well. It was pointed out that large ν densities in the deepest stellar regions can result in significant coherent ν - ν forward scatterings [5, 6]. A few years ago it was discovered that ν self-interactions can give rise to collective ν flavor oscillations inside the SN [7–9] (see [10] for a recent review). The most important observational consequence of this collective behavior is a swap of the ν_e and $\bar{\nu}_e$ spectra with the non-electron ν_x and $\bar{\nu}_x$ spectra in certain energy ranges [11, 12]. It has been argued that “spectral splits” at the edge of each swap interval would be observable in the high-statistics ν signal from the next galactic SN, allowing to get crucial information about the unknown ν mass ordering (see, e.g., [13]).

Self-induced oscillation effects crucially depend on the inner boundary conditions fixed for the further flavor evolution. Indeed, these non-linear flavor conversions are associated to instabilities in the flavor space, that develop around the crossing points in the energy spectra of the different ν species (where $F_{\nu_e} = F_{\nu_x}$ and $F_{\bar{\nu}_e} = F_{\bar{\nu}_x}$) [12]. The number and the position of the crossing points depend on the ordering of the original SN ν fluxes. Since this latter can change during the different post-bounce stages, significant temporal variations are expected in the pattern of the spectral splits [12, 14, 15]. An im-

portant layer of complication in this description is associated to the the current-current nature of the ν - ν weak-interaction Hamiltonian. This implies that the interaction energy between neutrinos of momenta \mathbf{p} and \mathbf{q} is proportional to $(1 - \mathbf{v}_p \cdot \mathbf{v}_q)$, where \mathbf{v}_p is the neutrino velocity [5, 6, 16]. In a non-isotropic medium this velocity-dependent term would not average to zero, producing a different refractive index for neutrinos propagating on different trajectories. This is the origin of the so-called “multi-angle effects,” which in some case can dramatically affect the development of the self-induced flavor conversions, producing a quick flavor decoherence [17, 18] or suppressing flavor conversions otherwise possible for an a isotropic neutrino emission [14, 15]. Moreover, it has been shown that the presence of the ordinary matter background would cause a multi-angle suppression of the collective oscillations, when the matter density dominates over the neutrino one [19]. This situation is expected to occur during the early times accretion phase [20–24].

The characterization of multi-angle effects is then a key-ingredient to obtain a realistic description of the self-induced neutrino flavor conversions. In this context, it is expected that the ν angular distributions at emission would play an important role in determining the ν - ν interaction strength. Until recently numerical simulations for the SN ν flavor conversions have been based on the so-called “bulb model” (see, e.g, [7, 11]), where ν ’s of different species are considered as emitted “half-isotropically” (i.e. with all outward-moving angular modes equally occupied and all the backward-moving modes empty) by a common spherical “neutrinosphere,” in analogy with a blackbody emission. However, realistic supernova simulations show that ν angular distributions at decoupling are far from being half-isotropic and, above all, are flavor-

dependent (see, e.g., [22, 25]). The presence of non-trivial angular distributions was claimed in [26] to produce a novel multi-angle instability in the self-induced flavor evolution of a toy model of ν gas. However, that conclusion was based on an analysis performed with a small number of angular modes, making challenging to rely on this claim to infer conclusions for the realistic SN ν case without a dedicated large-scale numerical study. Triggered also by this warning, in [1] we performed numerical simulations of the self-induced flavor conversions with non-trivial ν angular distributions, finding remarkable effects on the flavor evolution. In particular, when flavor-dependent angular distributions lead to crossing points in the angular spectra of different ν species, a new multi-angle instability can develop, in analogy to the known instability triggered by crossing points in the energy domain. We find cases in which this multi-angle instability can shift the onset of the flavor conversions toward low-radii and produce a smearing of the splitting features found with trivial ν emission models. In order to achieve a semi-analytical understanding of the phenomenon, in that Letter we proposed to apply to our problem the linearized stability analysis recently worked out in [27]. By seeking an exponentially growing solution in the eigenvalue equations associated with the linearized equations of motion for the neutrino ensemble, this method allowed us to determine the onset of the flavor conversions. In a specific scenario, we compared the growth of this mode in the half-isotropic case with different cases with non-trivial ν angular distributions, finding a significant enhancement of the instability in these latter cases.

The purpose of this follow-up work is to take a closer look to the multi-angle instability, triggered by non-trivial angular distributions. In particular we aim to use the stability analysis to perform an investigation on the dependence of this effect on the initial SN ν flux ordering, and on the ν mass hierarchy. Here is the plan of our work. In Sec. II we introduce the setup for the flavor-stability analysis, describing the non-linear equations for the ν flavor evolution in SNe, and the consistency equations coming from their linearization. In Sec. III we present our models for the supernova neutrino emission for cases with a different flux ordering and angular distributions. For these different cases we show the results of the stability analysis in the two neutrino mass hierarchies. Finally in Sec. IV we comment on our results and we conclude.

II. SETUP OF THE STABILITY ANALYSIS

A. Equations of motion

Our main goal is to perform a numerical stability analysis for the cases studied in [1]. Therefore, we use the same setup followed in that paper. In particular, we work in a two-flavor oscillation scenario, associated to the atmospheric mass-square difference $\Delta m_{\text{atm}}^2 = 2 \times 10^{-3}$ eV² and with the small (matter suppressed) in-medium

mixing $\Theta = 10^{-3}$. Since we aim at isolating the effect of the multi-angle instability, associated with ν non-trivial angular distributions, we assume in the following that self-induced flavor conversions are not matter suppressed (as expected instead at $t \lesssim 1$ s after the core bounce), ignoring the ordinary matter background in the equations of motion.

If we denote with ϑ_r the angle of a given neutrino trajectory with respect to the radial direction, flux conservation implies that it will depend on the radial coordinate r even for straight line propagation (as we consider here). It is thus convenient to parameterize every angular mode in terms of its emission angle ϑ_R relative to the radial direction of the neutrinosphere, that here we schematically fix at $R = 10$ km. For simplicity, we neglect possible residual scatterings that could affect ν 's after the neutrinosphere, producing a small “neutrino halo” that would broaden the ν angular distributions [28]. Indeed, it is expected that this effect may be relevant only at early times, where self-induced conversions would be matter suppressed [24]. For a half-isotropic distribution the occupation numbers are distributed as $dn/d\cos\vartheta_R = \text{const.}$, or equivalently the radial fluxes are distributed as $d\Phi/d\cos\vartheta_R \propto \cos\vartheta_R$ [18]. A further simplification is obtained if one labels the different angular modes in terms of the variable $u = \sin^2\vartheta_R$, as in [18, 27]. Note that for an half-isotropic emission at the neutrinosphere the ν angular distribution of the radial fluxes is a box spectrum in $0 \leq u \leq 1$, since $d\cos\vartheta_R/du \propto (\cos\vartheta_R)^{-1}$ which cancels the $\cos\vartheta_R$ dependence previously mentioned. At a radius r , the radial velocity of a mode with angular label u is $v_{u,r} = (1 - uR^2/r^2)^{1/2}$ [18]. Following [27], we write the equations of motion for the flux matrices $\Phi_{E,u}$ as function of the radial coordinate. The diagonal $\Phi_{E,u}$ elements are the ordinary number fluxes $F_{\nu_\alpha}(E, u)$ integrated over a sphere of radius r . We normalize the flux matrices to the total $\bar{\nu}_e$ number flux $N_{\bar{\nu}_e}$ at the neutrinosphere. Conventionally, we use negative E and negative number fluxes for anti-neutrinos. The off-diagonal elements, which are initially zero, carry a phase information due to flavor mixing. Then, the equations of motion read [27, 29]

$$i\partial_r \Phi_{E,u} = [H_{E,u}, \Phi_{E,u}] \quad (1)$$

with the Hamiltonian [5, 6, 27, 29]

$$H_{E,u} = \frac{1}{v_u} \frac{M^2}{2E} + \frac{\sqrt{2}G_F}{4\pi r^2} \int_{-\infty}^{+\infty} dE' \int_0^1 du' \left(\frac{1 - v_u v_{u'}}{v_u v_{u'}} \right) \Phi_{E',u'} \quad (2)$$

in which we neglected matter effects. The matrix M^2 of neutrino mass-squares causes vacuum flavor oscillations and the term at second lines represents the ν - ν refractive term. In particular, the factor proportional to the neutrino velocity $v_{u,r}$ in the ν - ν interaction term implies “multi-angle” effects for neutrinos moving on different

trajectories [5–7, 29]. In order to properly simulate numerically this effect one needs to follow a large number [$\mathcal{O}(10^3)$] of interacting ν modes.

B. Stability conditions

In order to perform the stability analysis we closely follow the prescriptions presented in [27] and summarized in the following. Firstly, we switch to the frequency variable $\omega = \Delta m_{\text{atm}}^2/2E$ so that $E(\omega) = |\Delta m_{\text{atm}}^2/2\omega|$ and we introduce the neutrino flux difference distributions $g_{\omega,u} \equiv g(\omega, u)$ defined as

$$g_{\omega,u} = \frac{|\Delta m_{\text{atm}}^2|}{2\omega^2} \times \left\{ \Theta(\omega) [F_{\nu_e}(E(\omega), u) - F_{\nu_x}(E(\omega), u)] + \Theta(-\omega) [F_{\nu_x}(E(\omega), u) - F_{\bar{\nu}_e}(E(\omega), u)] \right\}, \quad (3)$$

normalized to the total $\bar{\nu}_e$ flux at the neutrinosphere. Whenever referring to numerical values for the variables ω, μ we shall implicitly quote them in km^{-1} , as appropriate for the SN case. Note that $g_{\omega,u}$ is defined also for negative ω , where it represents the difference of fluxes in the antineutrino sector in the opposite ordering. Then, we write the flux matrices in the form [27]

$$\Phi_{\omega,u} = \frac{\text{Tr } \Phi_{\omega,u}}{2} + \frac{g_{\omega,u}}{2} \begin{pmatrix} s_{\omega,u} & S_{\omega,u} \\ S_{\omega,u}^* & -s_{\omega,u} \end{pmatrix}, \quad (4)$$

where $\text{Tr } \Phi_{\omega,u}$ is conserved and then irrelevant for the flavor conversions, and the initial conditions for the “swapping matrix” in the second term on the right-hand side are $s_{\omega,u} = 1$ and $S_{\omega,u} = 0$. Self-induced flavor transitions start when the off-diagonal term $S_{\omega,u}$ exponentially grows.

In the small-amplitude limit $|S_{\omega,u}| \ll 1$, and at far distances from the neutrinosphere $r \gg R$, the linearized evolution equations for $S_{\omega,u}$ in inverted mass hierarchy (IH, $\Delta m_{\text{atm}}^2 < 0$) assume the form [27]

$$\begin{aligned} i\partial_r S_{\omega,u} &= (\omega + u\epsilon\mu)S_{\omega,u} \\ &- \mu \int du' d\omega' (u + u') g_{\omega',u'} S_{\omega',u'} , \end{aligned} \quad (5)$$

where

$$\epsilon = \int du \ d\omega \ g_{\omega,u} , \quad (6)$$

quantifies the “asymmetry” of the neutrino spectrum, normalized to the total $\bar{\nu}_e$ number flux. The ν - ν interaction strength is given by

$$\begin{aligned} \mu &= \frac{\sqrt{2}G_F N_{\bar{\nu}_e}}{4\pi r^2} \frac{R^2}{2r^2} \\ &= \frac{3.5 \times 10^5}{r^4} \left(\frac{L_{\bar{\nu}_e}}{10^{52} \text{ erg/s}} \right) \left(\frac{15 \text{ MeV}}{\langle E_{\bar{\nu}_e} \rangle} \right) \left(\frac{R}{10 \text{ km}} \right)^2 . \end{aligned}$$

One can write the solution of the linear differential equation [Eq. (5)] in the form $S_{\omega,u} = Q_{\omega,u} e^{-i\Omega r}$ with complex frequency $\Omega = \gamma + i\kappa$ and eigenvector $Q_{\omega,u}$. A solution with $\kappa > 0$ would indicate an exponential increasing $S_{\omega,u}$, i.e. an instability. The solution of Eq. (5) can then be recast in the form of an eigenvalue equation for $Q_{\omega,u}$. Splitting this equation into its real and imaginary parts one arrives at two real equations that have to be satisfied [27]

$$\begin{aligned} (J_1 - \mu^{-1})^2 &= K_1^2 + J_0 J_2 - K_0 K_2 , \\ (J_1 - \mu^{-1}) &= \frac{J_0 K_2 + K_0 J_2}{2K_1} , \end{aligned} \quad (7)$$

where

$$\begin{aligned} J_n &= \int d\omega du g_{\omega,u} u^n \frac{\omega - \omega^*}{(\omega - \omega^*)^2 + \kappa^2} , \\ K_n &= \int d\omega du g_{\omega,u} u^n \frac{\kappa}{(\omega - \omega^*)^2 + \kappa^2} , \end{aligned} \quad (8)$$

and we introduced the *resonant frequency*

$$\omega^*(\gamma) = \gamma - u\epsilon\mu . \quad (9)$$

A flavor instability is present whenever Eqs. (7) admit a solution (γ, κ) . When an instability occurs, for a given angular mode u_0 the function $|Q_{\omega,u_0}|$ is a Lorentzian [12], centered around ω^* , with a width κ . Finally, we remind that the consistency equations in the normal mass hierarchy (NH) case ($\Delta m_{\text{atm}}^2 > 0$) are obtained simply changing the sign of $g_{\omega,u}$ in Eqs. (8) [27].

III. STABILITY ANALYSIS FOR DIFFERENT MODELS

A. Models for supernova neutrino emission

In order to perform our stability analysis we have to fix a neutrino emission model. Since our main goal is to explore in more detail the numerical findings presented in [1], in the following we refer to the cases discussed in that work. We remark that energy and angular distributions of SN ν 's entering $F_{\nu_\alpha}(E, u)$ are not independent of each other. However, schematically we assume that the angular distributions are energy independent. Then, we can factorize the ν flux of each flavor as $F_{\nu_\alpha}(E, u) = N_{\nu_\alpha} \times \varphi_{\nu_\alpha}(E) \times U_{\nu_\alpha}(u)$. The ν number $N_{\nu_\alpha} = L_{\nu_\alpha} / \langle E_{\nu_\alpha} \rangle$ is expressed in terms of the ν luminosity L_{ν_α} and of the ν average energy $\langle E_{\nu_\alpha} \rangle$ of the different species. The function $\varphi_{\nu_\alpha}(E)$ is the normalized ν energy spectrum ($\int dE \varphi_{\nu_\alpha}(E) = 1$) and $U_{\nu_\alpha}(u)$ is the normalized angular distribution ($\int du U_{\nu_\alpha}(u) = 1$).

We parametrize the energy spectrum as in Ref. [30]

$$\varphi(E) = \frac{(1+\alpha)^{1+\alpha}}{\Gamma(1+\alpha)} \frac{E^\alpha}{\langle E_\nu \rangle^{\alpha+1}} \exp \left[-\frac{(1+\alpha)E}{\langle E_\nu \rangle} \right] , \quad (10)$$

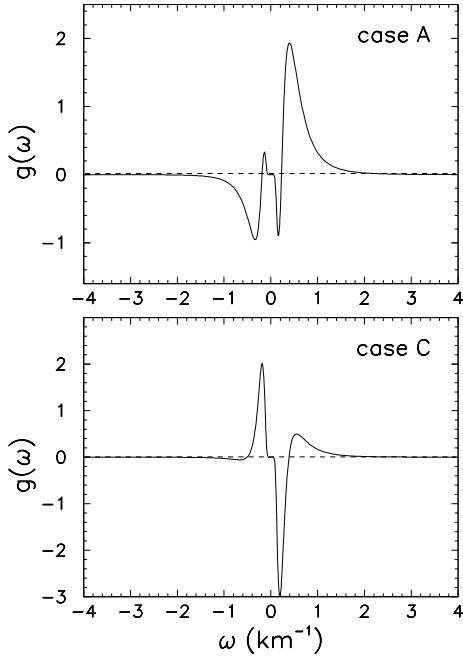


FIG. 1: Spectrum $g(\omega)$ for the case \mathcal{A} (upper panel) and \mathcal{C} (lower panel).

where we fix the spectral parameter to $\alpha = 3$ for all species. Following [1], we fix the neutrino average energies at

$$(\langle E_{\nu_e} \rangle, \langle E_{\bar{\nu}_e} \rangle, \langle E_{\nu_x} \rangle) = (12, 15, 18) \text{ MeV} . \quad (11)$$

Concerning the possible ν flux ordering we consider two cases. As representative of the accretion phase (labelled as case \mathcal{A}), we take

$$N_{\nu_e} : N_{\bar{\nu}_e} : N_{\nu_x} = 1.50 : 1.00 : 0.62 , \quad (12)$$

corresponding to an asymmetry parameter $\epsilon = 0.50$ in Eq. (6). Instead, as representative of the cooling phase, dubbed case \mathcal{C} , we choose

$$N_{\nu_e} : N_{\bar{\nu}_e} : N_{\nu_x} = 1.13 : 1.00 : 1.33 , \quad (13)$$

giving $\epsilon = 0.13$.

In Figure 1 we show the function $g_\omega = \int du g_{\omega,u}$ for the case \mathcal{A} (upper panel) and for the case \mathcal{C} (lower panel). Both spectra present three crossing points, where $g_\omega = 0$, so naively one would expect similar instability conditions in these two cases. However, as we will discuss in the following, the instabilities in these two cases are significantly different.

Concerning the neutrino angular distributions, we use the simple toy model introduced in [1] to capture the main deviations with respect to the half-isotropic bulb model, where $U_{\nu_\alpha} = 1$ for all the ν species. In particular, we choose forward-peaked distributions $U_{\nu_\alpha}(u) \propto (1-u)^{\beta_\alpha/2}$. For simplicity in the following we assume $U_{\nu_e} = U_{\bar{\nu}_e}$ and we refer to these cases:

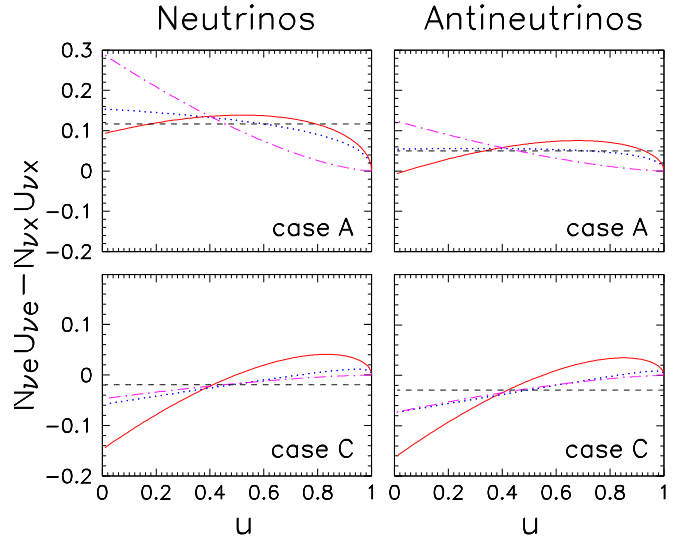


FIG. 2: Difference of the energy-integrated angular spectra $N_{\nu_e} U_{\nu_e}(u) - N_{\nu_x} U_{\nu_x}(u)$ for ν 's (left panels) and $\bar{\nu}$'s (right panels) for the case \mathcal{A} (upper panels) and \mathcal{C} (lower panels). The different curves correspond to $\beta_e = \beta_x = 0.0$ (dashed curves), $\beta_e = 1.0, \beta_x = 1.5$ (dotted curves), $\beta_e = 1.0, \beta_x = 3.0$ (continuous curves), $\beta_e = 3.0, \beta_x = 3.0$ (dash-dotted curves).

- $(\beta_e = \beta_x = 0.0)$,
- $(\beta_e = 1.0, \beta_x = 1.5)$,
- $(\beta_e = 1.0, \beta_x = 3.0)$,
- $(\beta_e = 3.0, \beta_x = 3.0)$.

In Figure 2 we plot the difference $N_{\nu_e} U_{\nu_e}(u) - N_{\nu_x} U_{\nu_x}(u)$ for ν 's (left panels) and the analogous one for $\bar{\nu}$'s (right panels) for the case \mathcal{A} (upper panels) and for the case \mathcal{C} (lower panels) for the four (β_e, β_x) cases. In the half-isotropic case $\beta_e = \beta_x = 0.0$, the differences of angular spectra do not present any crossing point in the angular variable, while in all the other cases, the spectra present a crossing point at $u = 1$ where $N_{\nu_e} U_{\nu_e}(u) = N_{\nu_x} U_{\nu_x}(u)$, and all the angular distributions U_{ν_α} vanish. In the case \mathcal{A} the angular distributions do not present other crossing points at finite u . Also for the $\bar{\nu}$'s in the $\beta_e = 1.0, \beta_x = 3.0$ case, the crossing point at finite u is so close to the edge of the spectrum at $u = 0$, that cannot be distinguished by it. Instead, in the case \mathcal{C} the (anti)neutrino angular spectra present also one crossing at finite $0 < u < 1$. In [1], we associated the speed-up of the multi-angle instability with the presence or absence of crossing points in the energy-integrated angular spectra. In the following, we shall confirm this explanation by performing an extensive stability analysis the different cases.

B. Case \mathcal{A}

The g_ω function for the case \mathcal{A} (Fig. 1 upper panel), presents three crossing points in the ω variable. According to what explained in [12] and confirmed by the stability analysis in [27], the instabilities that trigger self-induced oscillations are associated to crossings with positive slope in IH and to crossings with negative slope in NH. Therefore, one would have expected in this case a single self-induced spectral swap around $\omega = 0$ in normal hierarchy, and two spectral swaps in IH around the two crossings at finite ω . However, as observed in many numerical simulations for flux ordering with $N_{\nu_e} > N_{\bar{\nu}_e} > N_{\nu_x}$, the flavor evolution presents only a broad swap around $\omega = 0$ in IH and no conversion in NH. Indeed, as discussed in [12], a narrowly spaced triple crossing can superficially act like a single one at $\omega = 0$.

Hence, we present only the results for the IH case where the instability is expected to occur. Let us discuss first the half-isotropic case $\beta_e = \beta_x = 0.0$. In the case of a single-crossing spectrum, if the consistency equations [Eqs. (7)] admit a solution, this is a unique (γ, κ) for a given μ , or equivalently radial location in the SN [27]. In Figure 3 we show the (γ, κ) solution as a function of r (dashed curves for the half-isotropic case). The onset of the flavor conversions occurs when κ starts to grow, i.e. at $r \simeq 90$ km. In order to compare this prediction with the numerical results of the integration of the equations of motion [Eqs. (1)-(2)], we represent in Figure 4 the integrated value of the z -component of the ν polarization vector P_z , that is related to the flavor content of the ensemble. The onset of the flavor conversions for the half-isotropic case (dashed curve) is in good agreement with expectations from the stability analysis.

We pass now to analyze the cases with other neutrino angular distributions presented in Sec. IIIA. Figure 3 shows that different non-trivial cases do not lead to major changes in the behavior of the solution (γ, κ) of Eq. (8). In particular, no enhancement in the value of κ is observable. This result is consistent with the numerical simulations of the flavor evolution (see Fig. 4) that does not show any significant change in the non-trivial cases with respect to the half-isotropic one. The stability analysis confirms that in absence of crossing points in the angular spectra, no new multi-angle instability is triggered by the non-trivial angular distributions *alone*. The only observable consequence of the non-trivial angular distributions is a shift in the onset in the flavor conversions toward smaller r . Since forward-peaked distributions receive mostly contributions from small values of u , the resonance condition in Eq. (9) can be satisfied at larger μ , i.e. at smaller r with respect to the half-isotropic case. This is consistent with the expectation that the ν - ν strength is weaker for forward-peaked distributions, making the system to become unstable earlier than in the half-isotropic case. In particular, we find as onset of the flavor conversions $r = 87$ km for the case with $\beta_e = 1.0, \beta_x = 1.5$, $r = 88$ km, for the case with

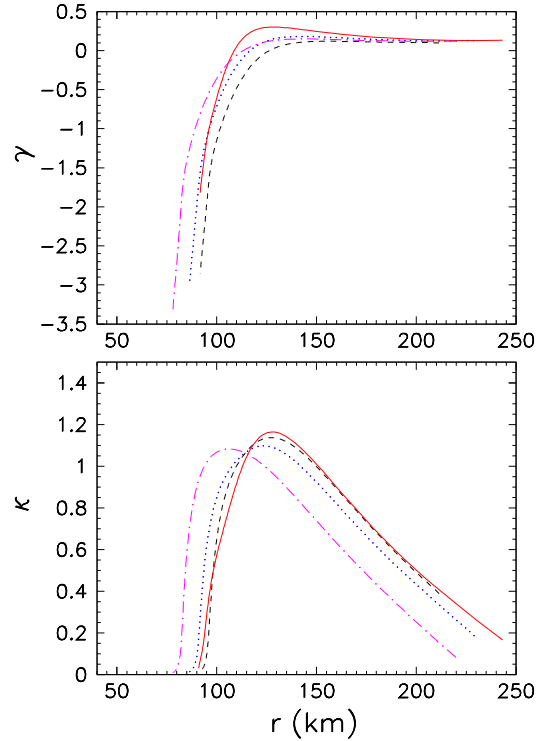


FIG. 3: Inverted mass hierarchy, case \mathcal{A} . Multi-angle eigenvalues $\gamma(r)$ and $\kappa(r)$. The different curves correspond to $\beta_e = \beta_x = 0.0$ (dashed curves), $\beta_e = 1.0, \beta_x = 1.5$ (dotted curves), $\beta_e = 1.0, \beta_x = 3.0$ (continuous curves), $\beta_e = 3.0, \beta_x = 3.0$ (dash-dotted curves).

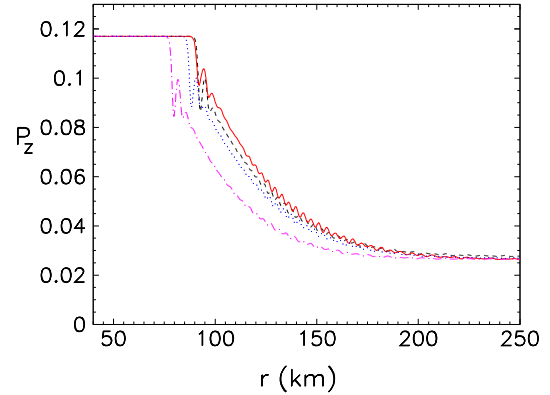


FIG. 4: Inverted mass hierarchy, case \mathcal{A} . Radial evolution of the integrated z -component of the neutrino polarization vector P_z . The different curves correspond to $\beta_e = \beta_x = 0.0$ (dashed curve), $\beta_e = 1.0, \beta_x = 1.5$ (dotted curve), $\beta_e = 1.0, \beta_x = 3.0$ (continuous curve), $\beta_e = 3.0, \beta_x = 3.0$ (dash-dotted curve).

$\beta_e = 1.0, \beta_x = 3.0$, and $r = 78$ km for $\beta_e = 3.0, \beta_x = 3.0$, consistently with what shown in Figure 4. Finally, we also checked that no effect is triggered in NH by the presence of non-trivial angular distributions.

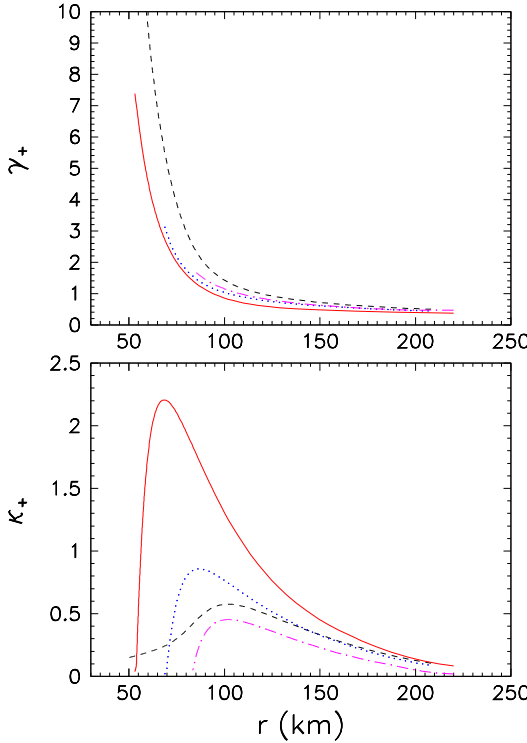


FIG. 5: Inverted mass hierarchy, case \mathcal{C} . Multi-angle eigenvalues $\gamma_+(r)$ and $\kappa_+(r)$. The different curves correspond to $\beta_e = \beta_x = 0.0$ (dashed curves), $\beta_e = 1.0, \beta_x = 1.5$ (dotted curves), $\beta_e = 1.0, \beta_x = 3.0$ (continuous curves), $\beta_e = 3.0, \beta_x = 3.0$ (dash-dotted curves).

C. Case \mathcal{C}

The g_ω spectrum for the case \mathcal{C} has been widely studied in the bulb model as representative of energy spectra with a flux ordering $N_{\nu_x} \gtrsim N_{\nu_e} \gtrsim N_{\bar{\nu}_e}$ and energy spectra with multiple crossing points leading to multiple splits around these points (see, e.g., [12, 14, 15]). Since we expect flavor instabilities in both the mass hierarchies, we discuss separately these two cases.

1. Inverted mass hierarchy

As discussed in [27], with spectra presenting three crossing points the consistency equations [Eq. (7)] admit a pair of solutions (γ_+, κ_+) and (γ_-, κ_-) (of course, if they admit a solution at all) for each value of μ , corresponding to negative and positive values of γ respectively. We show in Fig. 5 and 6 the functions $(\gamma_+(r), \kappa_+(r))$ and $(\gamma_-(r), \kappa_-(r))$, respectively, for the different angular distributions discussed before. A comparison between these two Figures reveals that κ_- is always smaller than κ_+ , meaning that the instability associated with κ_- will be always sub-leading. Therefore, in the following it suffices to discuss only the (γ_+, κ_+) solution. In the half-isotropic case $\beta_e = \beta_x = 0$ (dashed curve) the κ_+ function presents

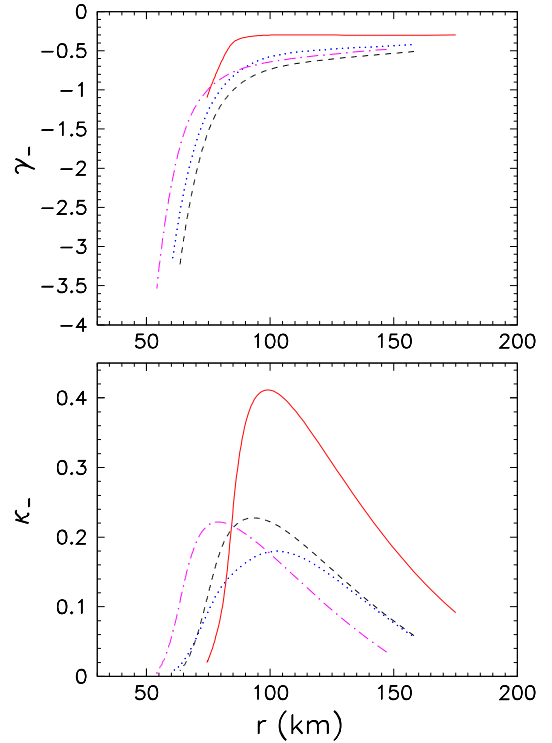


FIG. 6: Inverted mass hierarchy, case \mathcal{C} . Multi-angle eigenvalues $\gamma_-(r)$ and $\kappa_-(r)$. The different curves correspond to $\beta_e = \beta_x = 0.0$ (dashed curves), $\beta_e = 1.0, \beta_x = 1.5$ (dotted curves), $\beta_e = 1.0, \beta_x = 3.0$ (continuous curves), $\beta_e = 3.0, \beta_x = 3.0$ (dash-dotted curves).

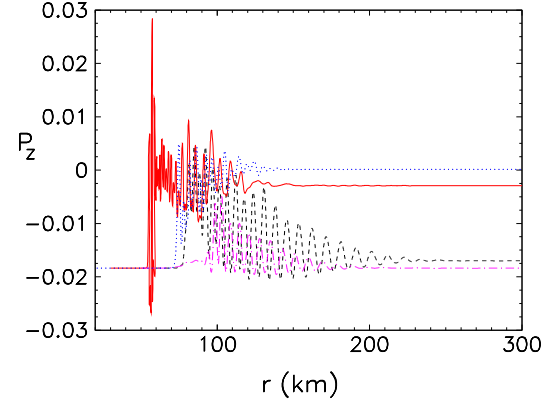


FIG. 7: Inverted mass hierarchy, case \mathcal{C} . Radial evolution of the integrated z -component of the neutrino polarization vector P_z . The different curves correspond to $\beta_e = \beta_x = 0.0$ (dashed curve), $\beta_e = 1.0, \beta_x = 1.5$ (dotted curve), $\beta_e = 1.0, \beta_x = 3.0$ (continuous curve), $\beta_e = 3.0, \beta_x = 3.0$ (dash-dotted curve).

a hump peaked around $r \simeq 100$ km and connected with a long tail at smaller r around $r \simeq 75$ km. This tail indicates that the system is in principle always unstable (also at very large values of μ). However, at large μ and γ_+ , the unstable frequency modes satisfying the resonance condition [Eq. (9)] are in the infrared region (i.e. $|\omega| > 4$),

where the g_ω spectrum is strongly suppressed. Therefore, they have no impact for the flavor conversions. The onset of the flavor conversions is then given by the connection between the hump and the tail at $r = 75$ km. This result is in agreement with what shown in the numerical calculation of P_z , shown in Fig. 7 (dashed curve).

When considering non-trivial angular distributions, the long tail in the κ_+ function observed in the half-isotropic case at small r now disappears. However, the presence of a non-isotropic angular distribution is not enough to produce an enhancement in the value of κ_+ . Conversely, in the flavor blind case $\beta_e = \beta_x = 3.0$ (dot-dashed curve) the instability is suppressed with respect to what has been seen in the half-isotropic case. Indeed, around the resonance energies [Eq. (9)], the integrals J_n and K_n in Eq. (7) are proportional to $\int du d\omega g_{\omega,u} u^n \kappa^{-2}$. Since with forward-peaked distributions these integral receive mostly contributions from small u , in order to satisfy the consistency equations [Eq. (7)] at a given μ , the corresponding κ_+ has to be smaller than in the half-isotropic case. In this case, flavor conversions start at $r = 80$ km.

A significant enhancement of the multi-angle instability occurs when ν angular spectra exhibit crossing points in u , as can be seen in the case with $\beta_e = 1.0, \beta_x = 1.5$ (dotted curve) and even more in the one with $\beta_e = 1.0, \beta_x = 3.0$ (continuous curve). In both cases the peak in κ_+ increases with respect to the half-isotropic case and also the hump broadens toward smaller r . Since κ_+ reaches a higher peak value, the width of the Lorentzian around an unstable frequency mode for a given angle u would be broad, implying a speed-up in the transitions. In particular, in the case of $\beta_e = 1.0, \beta_x = 1.5$ flavor conversions start around $r \simeq 70$ km, while in the case with $\beta_e = 1.0, \beta_x = 3.0$ around $r \simeq 55$ km, in agreement with the numerical results shown in Fig. 7.

In conclusion, we remark that SN ν spectra with multiple crossing points in the energy domain can exhibit flavor conversions at very large μ in a single-angle scheme [31]. Multi-angle effects in a half-isotropic situation suppress the instability at large neutrino densities [14, 31]. However, the stability analysis and our numerical simulations tell us that this stabilization effect is not a generic situation. Indeed, allowing for crossing points also in the angular spectra, flavor conversions can start much earlier than in the half-isotropic case.

2. Normal mass hierarchy

We finally pass to analyze the normal mass hierarchy case. Also here, we expect that the consistency equations [Eq. (7)] admit a pair of solutions (γ_+, κ_+) and (γ_-, κ_-) for each value of μ , that we represent in function of r in Fig. 8 and 9 respectively. The two imaginary parts of the eigenvalues, κ_+ and κ_- can assume comparable values, differently from the IH case. Whether κ_+ or κ_- plays the dominant role in triggering the flavor conversions will de-

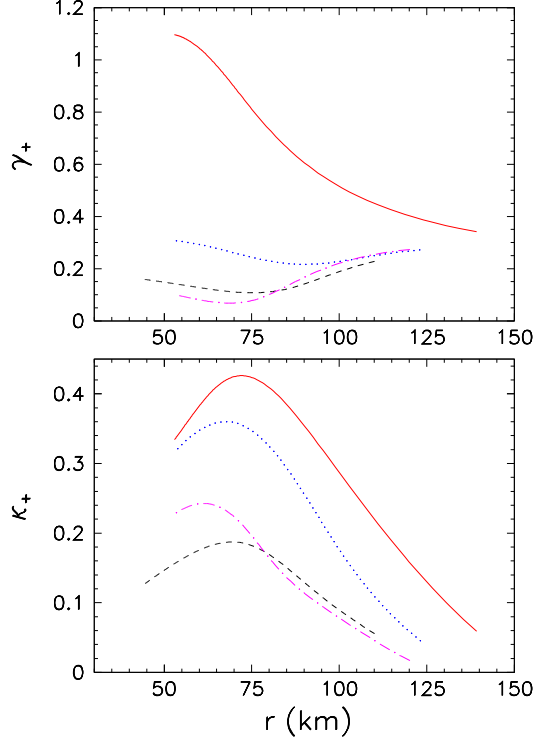


FIG. 8: Normal mass hierarchy, case \mathcal{C} . Multi-angle eigenvalues $\gamma_+(r)$ and $\kappa_+(r)$. The different curves correspond to $\beta_e = \beta_x = 0.0$ (dashed curves), $\beta_e = 1.0, \beta_x = 1.5$ (dotted curves), $\beta_e = 1.0, \beta_x = 3.0$ (continuous curves), $\beta_e = 3.0, \beta_x = 3.0$ (dash-dotted curves).

pend on the specific case. Starting with the half-isotropic case ($\beta_e = \beta_x = 0.0$, dashed curves) we see that both the functions κ_+ and κ_- present long tails extending at small r . However, κ_+ is always smaller than 0.2, while κ_- reaches a peak value ~ 0.6 at $r \simeq 105$ km. Therefore, the onset of the flavor conversions will be associated to κ_- , and as usual is determined by the connection of the hump with the tail of the function, i.e. at $r \simeq 80$ km, in agreement with the numerical evolution of P_z shown in Fig. 10 (dashed curve for the $\beta_e = \beta_x = 0.0$ case). In the flavor-blind case with $\beta_e = \beta_x = 3.0$ (dash-dotted curves) the dominant instability is again the one associated with κ_- that can reach as peak value ~ 0.5 at $r \simeq 105$ km. We note that in this case $\kappa_-(r)$ has no tail, terminating abruptly at $r \simeq 80$ km, while $\kappa_+(r)$ extends toward lower r reaching a almost constant value ~ 0.2 . The predicted onset of the flavor conversions can then be located at $r \simeq 80$ km. We see the corresponding numerical evolution in Fig. 10 (dash-dotted curve) starts at a slight larger radius, i.e. $r \simeq 90$ km. This delay is probably due to the time needed by the instability to grow significantly after it starts. This is related to the value of κ_- that is relatively small in this case. In the case $\beta_e = 1.0, \beta_x = 1.5$ (dotted curves) κ_- is further reduced with respect to the previous cases, while κ_+ is enhanced. Both the functions have a similar peak ~ 0.35 , but κ_+

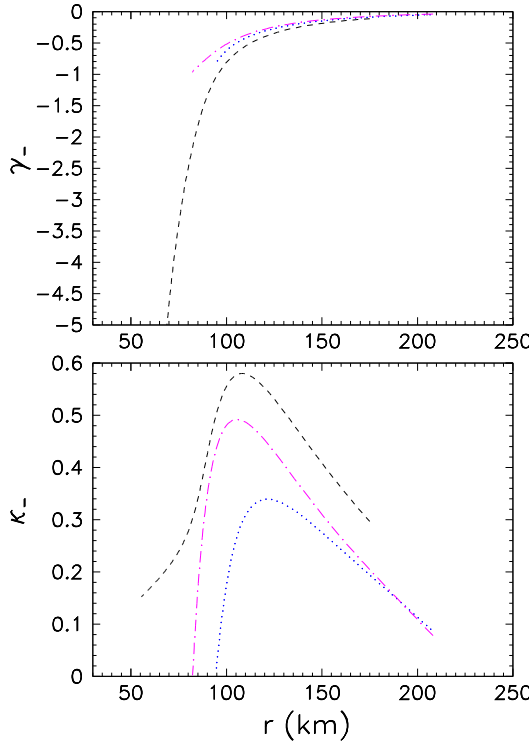


FIG. 9: Normal mass hierarchy, case \mathcal{C} . Multi-angle eigenvalues $\gamma_-(r)$ and $\kappa_-(r)$. The different curves correspond to $\beta_e = \beta_x = 0.0$ (dashed curves), $\beta_e = 1.0, \beta_x = 1.5$ (dotted curves), $\beta_e = 1.0, \beta_x = 3.0$ (continuous curves), $\beta_e = 3.0, \beta_x = 3.0$ (dash-dotted curves).

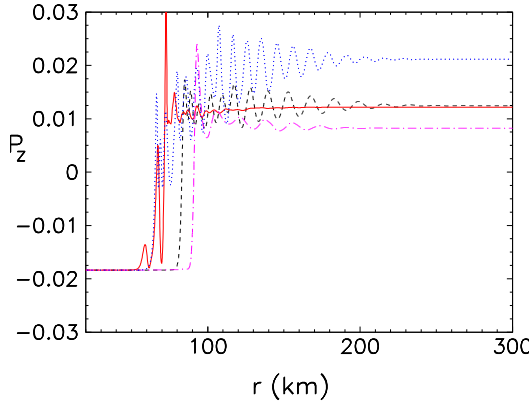


FIG. 10: Normal mass hierarchy, case \mathcal{C} . Radial evolution of the integrated z -component of the neutrino polarization vector P_z . The different curves correspond to $\beta_e = \beta_x = 0.0$ (dashed curve), $\beta_e = 1.0, \beta_x = 1.5$ (dotted curve), $\beta_e = 1.0, \beta_x = 3.0$ (continuous curve), $\beta_e = 3.0, \beta_x = 3.0$ (dash-dotted curve).

has a longer tail with a value close to the peak one, while κ_- abruptly drops at zero for $r \simeq 95$ km. Therefore, in this case the onset is determined by κ_+ . Since the unstable frequencies, determined by the resonance condition [Eq. (9)] would be in the infrared range (i.e. $\omega > 4$) for $\mu > 50$, the onset of relevant flavor conversions cor-

responds to this value of μ , i.e. $r \simeq 65$ km, as visible in the numerical evolution (dotted curve). Finally, in the case $\beta_e = 1.0, \beta_x = 3.0$ (continuous curve), the instability associated with κ_- disappears, while the one associated with κ_+ is further enhanced, reaching as peak value ~ 0.4 . This time the resonance condition reaches infrared frequency modes for $\mu \gtrsim 27$, corresponding to an onset of the flavor conversions at $r \lesssim 77$ km. Note that in this case the numerical evolution (continuous curve) the P_z starts to vary earlier, around $r = 55$ km, but it rises significantly only at $r \gtrsim 70$ km, as predicted by the stability analysis. This can be interpreted as follows: in the latter two cases, since the κ_- function presents a rather flat behavior in μ , the determination of the onset of the flavor conversions is less accurate. Indeed, also the numerical evolution in Fig. 10 shows that the P_z -component presents a slower rise time at the onset of the conversions.

IV. CONCLUSIONS

Self-induced flavor conversions for SN neutrinos are associated to instabilities in the flavor space. Recently, a linearized stability analysis of the SN ν equations of motion has been proposed as diagnostic tool to track the emergence of these instabilities [27]. In our work we have applied this technique to study the multi-angle instability associated with non-trivial neutrino angular distributions, extending the results presented in [1] to different SN ν flux orderings and ν mass hierarchies. We confirm that enhanced instabilities can occur, when the angular spectra present crossing points. Also, the onset of the flavor conversions typically shifts toward small radii, with respect to the half-isotropic case.

We cannot but emphasize that neutrino angular distributions should be taken into account in supernova neutrino phenomenological studies. For example, as pointed out in [1], one can expect a smearing of the splitting features observed in the half-isotropic case, with resulting ν fluxes showing less significant spectral differences. This tendency toward spectral equalization would challenge the detection of further oscillation signatures, like the ones associated with the Earth crossing of SN ν 's (see, e.g., [32, 33]). On the other hand, a sufficiently low-radii onset on the flavor conversions might imply an interesting impact on the r -process nucleosynthesis in SNe [34]. Eventually, if ν oscillations develop too close to the neutrinosphere, they might invalidate the ν transport paradigm in SNe that ignores ν conversions.

It is clear that future, state-of-the-art predictions of the neutrino flavor evolution in SNe would require as accurate as possible input from hydrodynamical simulations, providing the flavor, angular, energy and time structure of the fluxes. Here we showed that a preliminary flavor stability analysis presents some key advantages over a brute force numerical integration. While such a perturbative analysis cannot be used to deduce the eventual fate of the neutrino ensemble in flavor space, it

can be useful to identify the situations where angular distributions play a role in the flavor evolution. Once these cases are identified, it would be mandatory to perform large scale numerical simulations of the complete flavor evolution in order to determine the final oscillated neutrino spectra. With current level of sophistication in SN simulations, we believe that such studies will be mandatory to achieve a better characterization of the non-linear neutrino flavor evolution during a stellar gravitational collapse and a more realistic description of the neutrino signal from a future galactic SN.

Acknowledgments

We acknowledge Nicolas Bourbaki for useful discussions. We thank Georg Raffelt and Irene Tamborra for reading the manuscript and for interesting comments on it. The work of A.M. was supported by the German Science Foundation (DFG) within the Collaborative Research Center 676 “Particles, Strings and the Early Universe”.

[1] A. Mirizzi and P. D. Serpico, “Instability in the dense supernova neutrino gas with flavor-dependent angular distributions,” *Phys. Rev. Lett.* **108**, 231102 (2012) [arXiv:1110.0022 [hep-ph]].

[2] G. G. Raffelt, “Physics Opportunities With Supernova Neutrinos,” *Prog. Part. Nucl. Phys.* **64**, 393 (2010).

[3] L. Wolfenstein, “Neutrino Oscillations In Matter,” *Phys. Rev. D* **17**, 2369 (1978); S. P. Mikheev and A. Yu. Smirnov, “Resonance Enhancement Of Oscillations In Matter And Solar Neutrino Spectroscopy,” *Yad. Fiz.* **42**, 1441 (1985) [Sov. J. Nucl. Phys. **42**, 913 (1985)].

[4] A. S. Dighe and A. Y. Smirnov, “Identifying the neutrino mass spectrum from the neutrino burst from a supernova,” *Phys. Rev. D* **62**, 033007 (2000) [hep-ph/9907423].

[5] J. Pantaleone, “Neutrino oscillations at high densities,” *Phys. Lett. B* **287**, 128 (1992).

[6] Y. Z. Qian and G. Fuller, “Neutrino-neutrino scattering and matter enhanced neutrino flavor transformation in Supernovae,” *Phys. Rev. D* **51**, 1479 (1995) [astro-ph/9406073].

[7] H. Duan, G. M. Fuller, J. Carlson and Y. Z. Qian, “Simulation of coherent non-linear neutrino flavor transformation in the supernova environment. I: Correlated neutrino trajectories,” *Phys. Rev. D* **74**, 105014 (2006) [astro-ph/0606616].

[8] S. Hannestad, G. G. Raffelt, G. Sigl and Y. Y. Y. Wong, “Self-induced conversion in dense neutrino gases: Pendulum in flavour space,” *Phys. Rev. D* **74**, 105010 (2006) [Erratum-ibid. D **76**, 029901 (2007)] [astro-ph/0608695].

[9] Y. Pehlivan *et al.*, “Invariants of Collective Neutrino Oscillations,” *Phys. Rev. D* **84**, 065008 (2011) [arXiv:1105.1182 [astro-ph.CO]].

[10] H. Duan, G. M. Fuller and Y. Z. Qian, “Collective Neutrino Oscillations,” *Ann. Rev. Nucl. Part. Sci.* **60**, 569 (2010) [arXiv:1001.2799 [hep-ph]].

[11] G. L. Fogli, E. Lisi, A. Marrone and A. Mirizzi, “Collective neutrino flavor transitions in supernovae and the role of trajectory averaging,” *JCAP* **0712**, 010 (2007) [arXiv:0707.1998 [hep-ph]].

[12] B. Dasgupta, A. Dighe, G. G. Raffelt and A. Y. Smirnov, “Multiple Spectral Splits of Supernova Neutrinos,” *Phys. Rev. Lett.* **103**, 051105 (2009) [arXiv:0904.3542 [hep-ph]].

[13] H. Duan, G. M. Fuller, J. Carlson and Y. Q. Zhong, “Neutrino Mass Hierarchy and Stepwise Spectral Swapping of Supernova Neutrino Flavors,” *Phys. Rev. Lett.* **99**, 241802 (2007) [arXiv:0707.0290 [astro-ph]].

[14] H. Duan and A. Friedland, “Self-induced suppression of collective neutrino oscillations in a supernova,” *Phys. Rev. Lett.* **106**, 091101 (2011) [arXiv:1006.2359 [hep-ph]].

[15] A. Mirizzi and R. Tomas, “Multi-angle effects in self-induced oscillations for different supernova neutrino fluxes,” *Phys. Rev. D* **84**, 033013 (2011) [arXiv:1012.1339 [hep-ph]].

[16] R. F. Sawyer, “The multi-angle instability in dense neutrino systems,” *Phys. Rev. D* **79**, 105003 (2009) [arXiv:0803.4319 [astro-ph]].

[17] G. G. Raffelt and G. Sigl, “Self-induced decoherence in dense neutrino gases,” *Phys. Rev. D* **75**, 083002 (2007) [hep-ph/0701182].

[18] A. Esteban-Pretel, S. Pastor, R. Tomas, G. G. Raffelt and G. Sigl, “Decoherence in supernova neutrino transformations suppressed by deleptonization,” *Phys. Rev. D* **76**, 125018 (2007) [arXiv:0706.2498 [astro-ph]].

[19] A. Esteban-Pretel, A. Mirizzi, S. Pastor, R. Tomas, G. G. Raffelt, P. D. Serpico and G. Sigl, “Role of dense matter in collective supernova neutrino transformations,” *Phys. Rev. D* **78**, 085012 (2008) [arXiv:0807.0659 [astro-ph]].

[20] S. Chakraborty, T. Fischer, A. Mirizzi, N. Saviano and R. Tomas, “No collective neutrino flavor conversions during the supernova accretion phase,” *Phys. Rev. Lett.* **107**, 151101 (2011) [arXiv:1104.4031 [hep-ph]].

[21] S. Chakraborty, T. Fischer, A. Mirizzi, N. Saviano and R. Tomas, “Analysis of matter suppression in collective neutrino oscillations during the supernova accretion phase,” *Phys. Rev. D* **84**, 025002 (2011) [arXiv:1105.1130 [hep-ph]].

[22] S. Sarikas, G. G. Raffelt, L. Hudepohl and H. -T. Janka, “Suppression of Self-Induced Flavor Conversion in the Supernova Accretion Phase,” *Phys. Rev. Lett.* **108**, 061101 (2012) [arXiv:1109.3601 [astro-ph.SR]].

[23] N. Saviano, S. Chakraborty, T. Fischer and A. Mirizzi, “Stability analysis of collective neutrino oscillations in the supernova accretion phase with realistic energy and angle distributions,” *Phys. Rev. D* **85**, 113002 (2012) [arXiv:1203.1484 [hep-ph]].

[24] S. Sarikas, I. Tamborra, G. Raffelt, L. Hudepohl and H. -T. Janka, “Supernova neutrino halo and the suppression of self-induced flavor conversion,” *Phys. Rev. D* **85**, 113007 (2012) [arXiv:1204.0971 [hep-ph]].

[25] C. D. Ott, A. Burrows, L. Dessart and E. Livne, “2D Multi-Angle, Multi-Group Neutrino Radiation-

Hydrodynamic Simulations of Postbounce Supernova Cores,” *Astrophys. J.* **685**, 1069 (2008) [arXiv:0804.0239 [astro-ph]].

[26] R. F. Sawyer, “Speed-up of neutrino transformations in a supernova environment,” *Phys. Rev. D* **72**, 045003 (2005). [hep-ph/0503013].

[27] A. Banerjee, A. Dighe and G. Raffelt, “Linearized flavor-stability analysis of dense neutrino streams,” *Phys. Rev. D* **84**, 053013 (2011) [arXiv:1107.2308 [hep-ph]].

[28] J. F. Cherry, J. Carlson, A. Friedland, G. M. Fuller and A. Vlasenko, “Neutrino scattering and flavor transformation in supernovae,” *Phys. Rev. Lett.* **108**, 261104 (2012) [arXiv:1203.1607 [hep-ph]].

[29] G. Sigl and G. Raffelt, “General kinetic description of relativistic mixed neutrinos,” *Nucl. Phys. B* **406**, 423 (1993).

[30] M. T. Keil, G. G. Raffelt and H. T. Janka, “Monte Carlo study of supernova neutrino spectra formation,” *Astrophys. J.* **590**, 971 (2003) [astro-ph/0208035].

[31] G. G. Raffelt, “Self-induced parametric resonance in collective neutrino oscillations,” *Phys. Rev. D* **78**, 125015 (2008) [arXiv:0810.1407 [hep-ph]].

[32] C. Lunardini and A. Y. Smirnov, “Supernova neutrinos: Earth matter effects and neutrino mass spectrum,” *Nucl. Phys. B* **616**, 307 (2001) [hep-ph/0106149].

[33] E. Borriello, S. Chakraborty, A. Mirizzi, P. D. Serpico and I. Tamborra, “(Down-to-)Earth matter effect in supernova neutrinos,” arXiv:1207.5049 [hep-ph].

[34] H. Duan, A. Friedland, G. C. McLaughlin and R. Surman, “The influence of collective neutrino oscillations on a supernova r-process,” *J. Phys. G* **38**, 035201 (2011) [arXiv:1012.0532 [astro-ph.SR]].